Superconductivity in general domains

Virginie Bonnaillie
Département de Mathématiques, UMR CNRS 8628, Bât 425,
Université Paris-Sud, 91405 Orsay Cedex, France
E-mail : Virginie.Bonnaillie@math.u-psud.fr

Abstract

Motivated by the superconductivity, we are interested in the fundamental state of the Schrödinger operator with magnetic field in a domain with corners. In this paper, we propose a numerical approach based on the finite elements method to determine the bottom of the spectrum of this operator in general domains. We improve the numerical results by using mesh-refinment techniques based on a posteriori error estimates developed in [6]. We also look at the monotonicity of the bottom of the spectrum in an angular sector according to the angle to complement the theoretical study of [5, 7].

1 Introduction

1.1 Physical motivation

A superconducting sample cooled below a certain critical temperature T_C allows the current to flow with no resistance and so could carry current with no loss, we say that it is in a "superconductor state". This characteristic can explain the increasing interest of the experimental engineering for studying this phenomenon. An other advantage of superconductors is the exclusion of any magnetic field, that is to say a superconductor sample will not allow a magnetic field to penetrate its interior. This effect, called the Meissner Effect, occurs only for relatively small magnetic field. If the magnetic field becomes too large, the sample loses its superconducting behavior by penetration of the external magnetic field, it is the "normal state".
We distinguish two kinds of superconductors. The first, called "Type I superconductor", goes from the normal state to the superconductor state with Meissner effect if the external magnetic field crosses a critical value called H_C by decreasing. The second, called "Type II superconductor", passes from the normal state to the superconductor state with Meissner effect by going through a "mixed state" where the sample is superconductor but the external magnetic field penetrates by some vortices. This phenomenon was described by the Ginzburg-Landau theory developed by De Gennes [14] and Tinkham [26].
We consider a type II cylindrical superconducting sample and we denote by $\Omega \subset \mathbb{R}^2$ the cross section and apply a magnetic field $\mathcal{H}$ along the cylindrical

axis. Then, up to normalization factors, the free energy writes

$$\mathcal{G}(\psi,\mathcal{A})=\frac{1}{2}\int_\Omega\left\{|(\nabla-i\kappa\mathcal{A})\psi|^2+\kappa^2|\mathrm{curl}\,\mathcal{A}-\mathcal{H}|^2+\frac{\kappa^2}{2}(|\psi|^2-1)^2\right\}dx. \quad (1.1)$$

The superconducting properties are described by the minimizers $(\psi,\mathcal{A})$ of this Ginzburg-Landau functional $\mathcal{G}$.
We consider Ω a curvilinear polygon whose vertex are denoted by $S_1,\ldots,S_N$ with corresponding angles $\alpha_1,\ldots,\alpha_N$. The complex-valued function ψ is the order parameter ; the magnitude $|\psi|^2$ gives the density of superconducting electrons and the phase determines the current flow. In the normal state, $\psi\simeq 0$ and in the superconducting state, $|\psi|\simeq 1$. The vector field $\mathcal{A}$ defined on $\mathbb{R}^2$ is the magnetic potential and $B=\mathrm{curl}\,\mathcal{A}$ is the induced magnetic field. Two parameters are needed in the free energy (1.1) : $\mathcal{H}$ is the intensity of the applied magnetic field, assumed to be constant. The characteristic of the sample κ is called the "Ginzburg-Landau parameter", equal to the ratio between the coherence length and the penetration depth. The type I superconductor corresponds to $\kappa<\frac{1}{\sqrt{2}}$, and type II to $\kappa>\frac{1}{\sqrt{2}}$. We now assume κ large.

We notice that the Ginzburg-Landau functional is gauge invariant since

$$\forall\phi\in H^2(\Omega),\ \mathcal{G}(\psi e^{i\kappa\phi},\mathcal{A}+\nabla\phi)=\mathcal{G}(\psi,\mathcal{A}). \quad (1.2)$$

Revelant physical quantities are gauge invariant : the magnitude $|\psi|^2$, the intensity of the magnetic field B, the energy $\mathcal{G}$ and the superconducting current $j:=-\frac{i}{2\kappa}(\overline{\psi}\nabla\psi-\psi\nabla\overline{\psi})-|\psi|^2\mathcal{A}$. We can easily see that when $\psi=0$ then $j=0$; this means that the superconductivity is destroyed and there is no supercurrent.

The critical points of the Ginzburg-Landau functional (1.1) are solutions of the following Euler equation (cf [17, 14]) where Γ' is the set of the boundary where the unit outward normal vector ν is well defined and with the notation $\mathrm{curl}^{\,2}\mathcal{A}=(\partial_2(\mathrm{curl}\,\mathcal{A}),-\partial_1(\mathrm{curl}\,\mathcal{A}))$

$$\left\{\begin{array}{rcll} -(\nabla-i\mathcal{A})^2\psi &=& \kappa^2(1-|\psi|^2)\psi, & \text{in } \Omega,\\ \mathrm{curl}^{\,2}\mathcal{A} &=& -\frac{i}{2\kappa}(\overline{\psi}\nabla\psi-\psi\nabla\overline{\psi})-|\psi|^2\mathcal{A}+\mathrm{curl}\,\mathcal{H}, & \text{in } \Omega,\\ \frac{\partial\psi}{\partial\nu}-i\kappa\mathcal{A}\psi\cdot\nu &=& 0, & \text{in } \Gamma',\\ \mathrm{curl}\,\mathcal{A}-\mathcal{H} &=& 0 & \text{in } \partial\Omega. \end{array}\right. \quad (1.3)$$

1.2 Link with the Schrödinger operator

The analysis of the Hessian of the functional $\mathcal{G}$ leads to estimate the fundamental state for the Neumann realization of the Schrödinger operator with intense magnetic field for which the superconductivity occurs. We define the sesquilinear form $a_{\mathcal{A},\Omega}$ in the form domain

$$H^1_{\mathcal{A}}(\Omega)=\{u\in L^2(\Omega)|\nabla_{\mathcal{A}}u\in(L^2(\Omega))^2\}\text{ with }\nabla_{\mathcal{A}}=\nabla-i\mathcal{A}, \quad (1.4)$$

by

$$a_{\mathcal{A},\Omega}(u,v)=\int_\Omega\nabla_{\mathcal{A}}u\cdot\overline{\nabla_{\mathcal{A}}v}\,dx,\ \forall u,v\in H^1_{\mathcal{A}}(\Omega). \quad (1.5)$$

The sesquilinear form $a_{\mathcal{A},\Omega}$ is semi-bounded from below and so admits a unique self-adjoint extension $P_{\mathcal{A},\Omega} := -\nabla^2_{\mathcal{A}}$ defined on the domain

$$\mathcal{D}^N(P_{\mathcal{A},\Omega}) := \{u \in H^1_{\mathcal{A}}(\Omega)|\ \nabla^2_{\mathcal{A}} u \in L^2(\Omega),\ \nu \cdot \nabla_{\mathcal{A}} u_{|\Gamma'} = 0\}.$$

Our goal is to determined the fundamental state for the operator $P_{\mathcal{A},\Omega}$. The weak formulation of this problem reads

$$\begin{array}{l} \text{Find } (\mu, u) \in \mathbb{R} \times H^1_{\mathcal{A}}(\Omega) \text{ with the smallest } \mu \text{ s.t.} \\ \forall v \in H^1_{\mathcal{A}}(\Omega), \left\{ \begin{array}{rcl} \int_\Omega \nabla_{\mathcal{A}} u \cdot \overline{\nabla_{\mathcal{A}} v} dx & = & \mu \int_\Omega u \overline{v} dx, \\ \int_\Omega |u|^2 dx & = & 1. \end{array} \right. \end{array} \tag{1.6}$$

Let us recalling the gauge invariance.

Proposition 1.1. *For any $\phi \in H^2(\Omega)$, the operators $P_{\mathcal{A},\Omega}$ and $P_{\mathcal{A}+\nabla\phi,\Omega}$ are unitary equivalent. Furthermore, (μ, u) is in the spectrum of $P_{\mathcal{A},\Omega}$ if and only if $(\mu, ue^{i\phi})$ is in the spectrum of $P_{\mathcal{A}+\nabla\phi,\Omega}$.*

Proof : Let $\phi \in H^2(\Omega)$, we define the unitary transform U from $\mathcal{D}^N(P_{\mathcal{A},\Omega})$ onto $\mathcal{D}^N(P_{\mathcal{A}+\nabla\phi,\Omega})$ by $Uu = e^{i\phi}u$ for all $u \in \mathcal{D}^N(P_{\mathcal{A},\Omega})$. Thus

$$U P_{\mathcal{A},\Omega} = P_{\mathcal{A}+\nabla\phi,\Omega} U. \tag{1.7}$$

The two operators are unitary equivalent and have therefore the same spectrum. □

Proposition 1.1 shows that the bottom of the spectrum of $P_{\mathcal{A},\Omega}$ depends only on the magnetic field and not on the magnetic potential. Then, we denote by $\mu(B,\Omega)$ the bottom of the spectrum of $P_{\mathcal{A},\Omega}$ for any potential $\mathcal{A}$ such that $\operatorname{curl}\mathcal{A} = B$. Furthermore, if $\mathcal{A}$ is a potential with constant magnetic field B, then the operator $P_{\mathcal{A},\Omega}$ has the same spectrum as $P_{B\mathcal{A}_0,\Omega}$ with the notations

$$\mathcal{A}_0 = \frac{1}{2}(x_2, -x_1). \tag{1.8}$$

Due to the min-max principle, $\mu(B,\Omega)$ is equal to

$$\mu(B,\Omega) = \inf_{u \in H^1_{\mathcal{A}}(\Omega), u \neq 0} \frac{\int_\Omega |(\nabla - i\mathcal{A})u|^2\ dx}{\int_\Omega |u|^2\ dx} \text{ for any } \mathcal{A} \text{ s. t. } \operatorname{curl}\mathcal{A} = B. \tag{1.9}$$

A lot of papers [15, 16, 17, 22, 23] deal with estimates of $\mu(B,\Omega)$ and localization of the fundamental state in regular domains ; particularly Helffer-Morame [15, 16] prove the localization of the fundamental state in the boundary and more precisely at points with maximum curvature. We want to carry on their analysis by determining the effects of a non regularity of the boundary. Some results are announced by the Physicists Brosens, Devreese, Fomin, Moshchalkov, Schweigert and Peeters in [11, 13, 25] but not proved. Jadallah [19, 20] and Pan [24] study the effect of the right corner and a more general theoretical analysis is proposed in [5, 7]. As illustrated in Figures 1 and 2, a partition of identity and a change of variables reduce the study of $P_{\mathcal{A},\Omega}$ for any curvilinear domain Ω to the study of three models operators

$$P_{\mathcal{A}_0,\mathbb{R}^2},\ P_{\mathcal{A}_0,\mathbb{R}\times\mathbb{R}^+} \text{ and } P_{\mathcal{A}_0,\Omega_\alpha}, \tag{1.10}$$

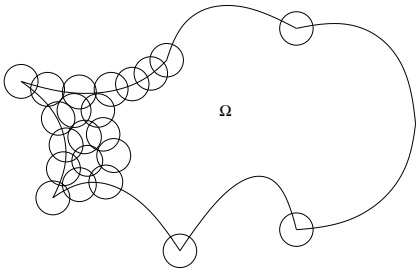

Figure 1: General curvilinear domain.

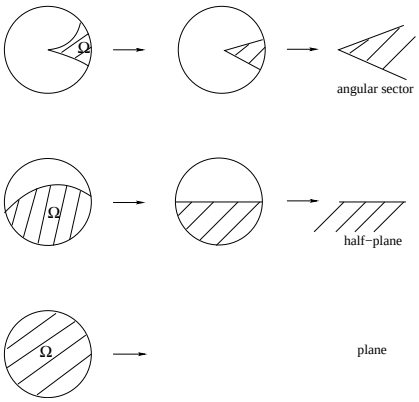

Figure 2: Models domains.

where $\Omega_\alpha := \left\{x \in \mathbb{R}^2 |\ x_1 > 0, |x_2| < \tan\frac{\alpha}{2}x\right\}$ is the angular sector defined for $\alpha \in]0, 2\pi]$. We denote more lightly by $\mu(\alpha) = \mu(1, \Omega_\alpha)$ the bottom of the spectrum of $P_{\mathcal{A}_0,\Omega_\alpha}$. Due to [5, 7], we know that the first eigenfunction of $P_{B\mathcal{A}_0,\Omega}$ is exponentially localized in corners S_j where $\mu(\alpha_j)$ is minimum. This present paper is more devoted to the numerical computation of $\mu(\alpha)$ and localization of the eigenfunction in any domain. For the numerical treatment of the problem, we restrict our study to potential $\mathcal{A}$ with constant magnetic field and, due to gauge invariance (Proposition 1.1), we assume that $\mathcal{A} = B\mathcal{A}_0$. The exponential localization in some points of the boundary makes the numerical treatment particularly ill conditioned and difficult.

This article is organized as follows. In Section 2, we first recall some easy invariance properties of $P_{\mathcal{A}_0,\Omega}$. These properties can explain in Section 2.3 why the standard method consisting in constructing the stiffness and mass matrices and computing the generalized eigenvalues, is unefficient for this problem. Section 2.4 proposes a robuster method respecting invariance properties. To know if we catch the solution with a good accuracy, Section 3 shows how we can use a mesh-refinement method coupled to a posteriori error estimates given in [6] to improve accuracy. We see the performance of this method by comparing it with the computations on uniform meshes. In the last Section 4, we use this method to compute $\mu(\alpha)$ and see its monotonicity according to the angle. We also test the robustness of this method on several domains having one corner with smallest angle or domain with one point with maximum curvature.

2 Numerical modelization

2.1 Invariance properties

We quickly present classical properties of the spectrum of $P_{B\mathcal{A}_0,\Omega}$. These properties can easily be justified by change of variables and construction of an unitary transformation.

Remark 2.1.

1. *Let Ω be a domain invariant under dilatation, then the spectrum of $P_{B\mathcal{A}_0,\Omega}$ is deduced from the spectrum of $P_{\mathcal{A}_0,\Omega}$ multiplied by B.*

2. *We denote by* $\Omega_t := \{y \in \mathbb{R}^2 | y - t \in \Omega\}$ *the domain deduced from* Ω *after translation by* t. *Then the operators* $P_{B\mathcal{A}_0,\Omega}$ *and* $P_{B\mathcal{A}_0,\Omega_t}$ *are unitary equivalent. Furthermore,* u *is an eigenvector for the operator* $P_{B\mathcal{A}_0,\Omega}$ *associated to the egenvalue* μ *if and only if* u_t *is an eigenvector associated to the eigenvalue* μ *for the operator* $P_{B\mathcal{A}_0,\Omega_t}$, *with* u_t *defined on* Ω_t *by*

$$u_t(y) := e^{i\frac{B}{2}y\wedge t}\ u(y-t). \tag{2.1}$$

3. *Let* $\Omega^\eta := \{(\rho,\phi) \in \mathbb{R}^2 |\ (\rho, \phi - \eta) \in \Omega\}$ *the domain deduced from* Ω *after a rotation of angle* η. *Then the two operators* $P_{B\mathcal{A}_0,\Omega}$ *and* $P_{B\mathcal{A}_0,\Omega^\eta}$ *have the same smallest eigenvalue and the eigenfunctions are deduced one from the other by a change of variables.*

2.2 Computation of a generalized eigenvalue

Let A and M be two positive definite hermitian matrices. We want to determine the smallest μ and a vector x such that

$$\left\{ \begin{array}{rcl} Ax & = & \mu Mx, \\ \langle Mx, x\rangle_{L^2(\Omega)} & = & 1. \end{array} \right. \tag{2.2}$$

The problem (2.2) consists in minimizing $\langle Ax, x\rangle_{L^2(\Omega)}$ with respect to the constraint $\langle Mx, x\rangle_{L^2(\Omega)} = 1$.

Proposition 2.2. *Let* x_0 *be a vector such that* $\langle Mx_0, x_0\rangle_{L^2(\Omega)} = 1$. *For any* $n \geq 0$, *we consider* w_n *the solution of the minimization problem*

$$\min_{w | \langle Mx_n, w\rangle_{L^2(\Omega)} = 0} \langle A(x_n + w), x_n + w\rangle_{L^2(\Omega)}\,. \tag{2.3}$$

Let us define

$$x_{n+1} := \frac{x_n + w_n}{\sqrt{\langle M(x_n + w_n), x_n + w_n\rangle_{L^2(\Omega)}}}. \tag{2.4}$$

Then, the vector x_n *is normalized with respect to* M, *the associated energy is decreasing, tending to a generalized eigenvalue of* (A, M) *denoted by* E_∞. *If the generalized eigenvalue* E_∞ *is simple, then* (x_n) *converges to a normalized eigenvector* x_∞ *for* E_∞ *; otherwise, there exists a subsequence of* (x_n) *which converges to a normalized eigenvector for* E_∞.

Proof : For $n \geq 0$, we consider the solution w_n of the minimization problem (2.3). Euler equation for the problem (2.3) leads to

$$A(x_n + w_n) = \langle A(x_n + w_n), x_n\rangle_{L^2(\Omega)}\, Mx_n. \tag{2.5}$$

Taking the scalar product of (2.5) with w_n, we easily deduce

$$\langle A(x_n + w_n), w_n\rangle_{L^2(\Omega)} = 0. \tag{2.6}$$

We now show that the energy associated to $x_n + w_n$ is less than the one of x_n. From the assumption on w_n, $\langle Mx_n, w_n\rangle_{L^2(\Omega)} = 0$ and we have

$$\frac{\langle A(x_n + w_n), x_n + w_n\rangle_{L^2(\Omega)}}{\langle M(x_n + w_n), x_n + w_n\rangle_{L^2(\Omega)}} \quad = \quad \frac{\langle A(x_n + w_n), x_n + w_n\rangle_{L^2(\Omega)}}{1 + \langle Mw_n, w_n\rangle_{L^2(\Omega)}}, \tag{2.7}$$

since x_n is normalized according M. According (2.6), we see that

$$\langle A(x_n + w_n), x_n + w_n \rangle_{L^2(\Omega)} = \langle Ax_n, x_n \rangle_{L^2(\Omega)} - \langle Aw_n, w_n \rangle_{L^2(\Omega)} . \tag{2.8}$$

Thus, definition (2.4) of x_{n+1}, Relations (2.7) and (2.8) lead to

$$\langle Ax_{n+1}, x_{n+1} \rangle_{L^2(\Omega)} \leq \langle Ax_n, x_n \rangle_{L^2(\Omega)} - \langle Aw_n, w_n \rangle_{L^2(\Omega)} . \tag{2.9}$$

By sommation on n in (2.9), we prove that the serie $\sum_n \langle Aw_n, w_n \rangle_{L^2(\Omega)}$ is convergent and so $\langle Aw_n, w_n \rangle_{L^2(\Omega)}$ and therefore w_n tend to 0 as $n \to \infty$.
The energy of (x_n) is decreasing, bounded from below by the smallest generalized eigenvalue for (A, M), so tends to a positive real number denoted by E_∞ as $n \to \infty$. The sequence (x_n) is bounded, then there exists a subsequence of (x_n) converging to a vector denoted by x_∞. Using (2.5), x_∞ is a normalized eigenvector for E_∞, and we particularly deduce that E_∞ is an eigenvalue. If the eigenvalue E_∞ is simple, then (x_n) tends to x_∞. Indeed, the sequence (x_n) has got at most two adherence values since an adherence value is an eigenfunction. But if (x_n) has two adherence values, it has at least a third one because $(x_{n+1} - x_n)$ tends to 0 when $n \to \infty$. □
Let us be more precise about the construction of w_n. We define the orthogonal projector Π_n on $(Mx_n)^\perp$ and can establish from (2.3) that

$$\Pi_n A \Pi_n w_n = -\Pi_n A x_n. \tag{2.10}$$

The matrix $\Pi_n A \Pi_n$ is hermitian and positive definite on $(Mx_n)^\perp$ and so we can determine w_n by a gradient conjugate method. This leads to the following algorithm

---

Algorithm 2.3 (Generalized eigenvalue)**.**

- *Let us give a number of iterations n_{max} and an accuracy level ε.*
- *Initialization : $\varepsilon_0 = 1$, $n = 0$, x_0 verifying $\langle Mx_0, x_0 \rangle_{L^2(\Omega)} = 1$ and $\mu_0 = \langle Ax_0, x_0 \rangle_{L^2(\Omega)}$.*
- *While $n < n_{max}$ and $\varepsilon_n > \varepsilon$:*

  1. *Construction of the projector $\Pi_n : w \mapsto w - \dfrac{\langle Mw, x_n \rangle_{L^2(\Omega)}}{||Mx_n||^2_{L^2(\Omega)}} Mx_n$. (we just need to compute $\Pi_n y$ for some y.)*
  2. *Determination of w_n such that $\Pi_n A \Pi_n w_n = -\Pi_n A x_n$ by a gradient conjugate method with accuracy ε and maximum iterations n_{max}.*
  3. *Construction of $x_{n+1} = \dfrac{x_n + w_n}{\sqrt{\langle M(x_n + w_n), x_n + w_n \rangle_{L^2(\Omega)}}}$.*
  4. *Computation of energy : $\mu_{n+1} = \langle Ax_{n+1}, x_{n+1} \rangle_{L^2(\Omega)}$.*
  5. *Computation of error : $\varepsilon_{n+1} = \max(|\mu_n - \mu_{n+1}|, ||x_n - x_{n+1}||)$.*
  6. *Increment $n = n + 1$.*

Remark 2.4. *Let us notice that each eigenvector is a critical point for Algorithm 2.3. Nevertheless, we hope that numerical errors make Algorithm 2.3 converge to the smallest eigenvalue.*

2.3 Standard method

We denote by $\mathcal{T}_h$ a triangulation of Ω and $\mathbb{P}^k(\mathcal{T}_h)$ or $\mathbb{P}^k$ the triangular elements based on polynomials of degree k. The weak formulation was recalled in (1.6) and the associated discrete formulation consists in finding $(\mu_h, u_h) \in \mathbb{R} \times \mathbb{P}^k(\mathcal{T}_h)$ such that μ_h is the smallest and

$$\int_\Omega |u_h|^2 \, dx = 1 \text{ and } \int_\Omega \nabla_{\mathcal{A}} u_h \cdot \overline{\nabla_{\mathcal{A}} v_h} dx = \mu_h \int_\Omega u_h \overline{v_h} dx, \ \forall v_h \in \mathbb{P}^k(\mathcal{T}_h). \quad (2.11)$$

The natural idea is to construct the mass and stiffness matrices. So, if we decompose u_h according the basis functions $(\phi_j)_j$, we have to determine coefficients $u_j \in \mathbb{C}$ and the smallest $\mu_h \in \mathbb{R}$ such that

$$\sum_j |u_j|^2 = 1 \text{ and } \forall k, \ \sum_j u_j \ \int_\Omega \nabla_{\mathcal{A}} \phi_j \cdot \overline{\nabla_{\mathcal{A}} \phi_k} \ dx = \mu_h \sum_j u_j \ \int_\Omega \phi_j \ \overline{\phi_k} \ dx. \quad (2.12)$$

We construct the matrices M and A by their coefficients computed by numerical integration and a quadrature formula with high order

$$M_{j,k} \simeq \int_\Omega \phi_j \overline{\phi_k} \ dx \quad \text{and} \quad A_{j,k} \simeq \int_\Omega \nabla_{\mathcal{A}} \phi_j \cdot \overline{\nabla_{\mathcal{A}} \phi_k} \ dx.$$

It is easily seen that the numerical problem deduced from (2.12) is to determine the smallest generalized eigenvalue μ_h for (A, M) and its eigenvector U such that

$$AU = \mu_h MU \text{ and } {}^tUMU = 1. \quad (2.13)$$

Remark 2.5. *Formulation (2.13) is not gauge invariant. Indeed, if u is piecewise polynomial, then $e^{i\phi}u$ is not for any linear ϕ and so is not in the discretization's space.*

We use Algorithm 2.3 to solve (2.13). We consider a mesh $\mathcal{T}_h^0$ of a domain Ω and construct meshes $\mathcal{T}_h^j$ deduced from $\mathcal{T}_h^0$ by a translation of vectors $\mathbf{t_j} = (j, 0)$ for $j = 1, 2$. So $\mathcal{T}_h^j$ is a mesh of the domain Ω^j deduced from Ω by translation of $\mathbf{t_j}$. We denote by (μ^j, u^j), (μ_h^j, u_h^j) respectively the solution of the continuous problem (1.6) and of the discrete problem (2.13) computed on each mesh $\mathcal{T}_h^j$ with the smallest μ^j and μ_h^j for $j = 0, 1, 2$. According to Remark 2.1, we must have for $j = 1, 2$

$$\left\{ \begin{array}{rcl} \mu^j & = & \mu^0, \\ u^j(x) & = & e^{i\frac{B}{2}x \wedge \mathbf{t_j}} u^0(x - \mathbf{t_j}), \ \forall x \in \Omega^j. \end{array} \right. \quad (2.14)$$

We consider two initial meshes with respectively 138 and 1328 elements. We apply a magnetic field with intensity equal to $B = 10$, 30, 50 Teslas. Table 1 gives the energy computed on each mesh.

The results partially presented in Figures 3 and 4 don't agree with Remark 2.1. The bad numerical results can be explained by the fact that a $\mathbf{t}$-translation generates phase oscillations due to the term $\frac{B}{2} x \wedge \mathbf{t}$ as explained in

B	Mesh with 138 elements			Mesh with 1328 elements		
	μ_h^0	μ_h^1	μ_h^2	μ_h^0	μ_h^1	μ_h^2
$B = 10$ Teslas	4.3306	4.2551	5.4980	4.1860	4.1810	4.2330
$B = 30$ Teslas	14.3868	18.1965	30.2870	12.6555	12.9483	20.3891
$B = 50$ Teslas	27.6519	43.7395	51.1149	21.3263	26.7383	47.5876

Table 1: Energy computed on translated meshes.

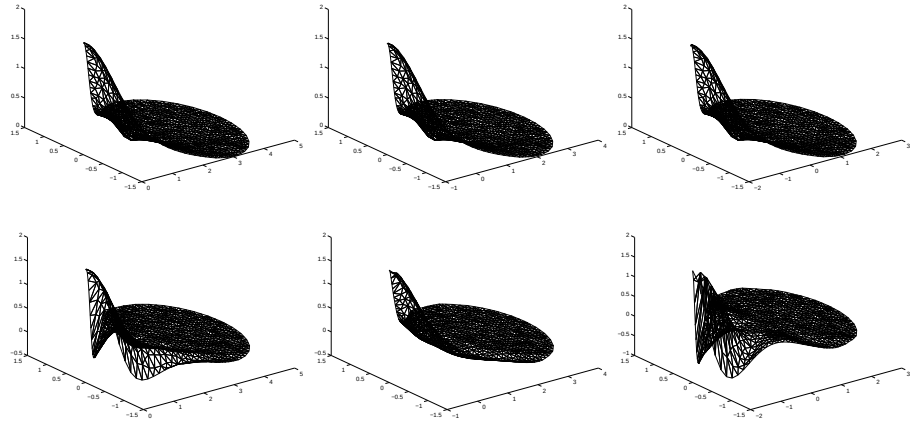

Figure 3: Modulus and real part of the fundamental state associated to translated meshes, $B = 10$ Teslas, mesh with 1328 elements.

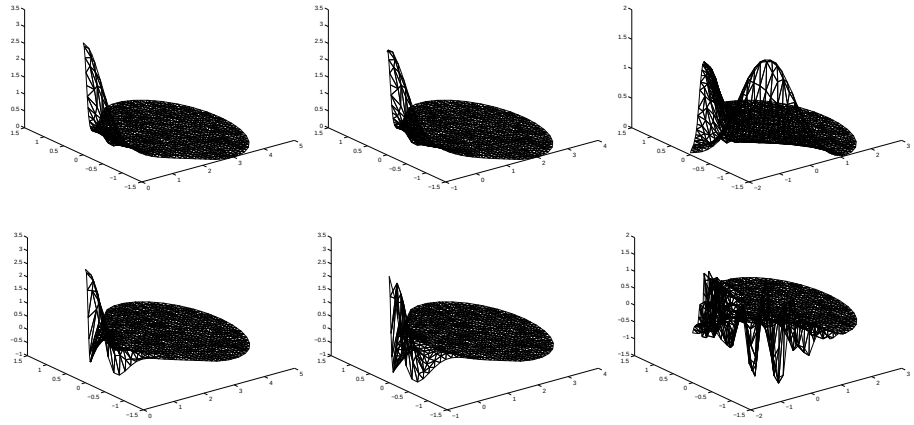

Figure 4: Modulus and real part of the fundamental state associated to translated meshes, $B = 30$ Teslas, mesh with 1328 elements.

(2.14). With a $\mathbb{P}^1(\mathcal{T}_h^j)$ discretization, a necessary condition to catch the oscillations obtained by the coefficient $e^{i\frac{B}{2}x\wedge\mathbf{t}}$ is that the size of the space step h must

be small compared to $\frac{1}{B|\mathbf{t}|}$. For a magnetic field equal to 10 Teslas, Figure 3 shows quite acceptable results since eigenvalues and moduli are close for every meshes. If the mesh is too coarse, then it is impossible to catch these oscillations. This phenomenon appears in Figure 4. As soon as the translation is too large or the magnetic fiel too big, then the fundamental state can't be determined accurately. Unfortunately, the condition $h < \frac{1}{B\mathbf{t}}$ is too much restrictive since it is easily violated when B or $\mathbf{t}$ increases.
Therefore this method does not respect invariance properties due to gauge transformation or translation of the domain and we have to find another numerical modelization. Furthermore, we expect the eigenfunction to be localized on the boundary, and more precisely on corners with smallest angle. This concentration leads us to use adaptive refinement mesh technique. Our new method not only must be gauge invariant, but also has to be compatible with mesh refinement techniques. As the phase plays an important role for a gauge transform or a domain translation, we look for a formulation using the phase.

2.4 A new approach of the problem

As we see in previous section, the standard method is unefficient to solve this numerical problem. Its weakness is due to its non gauge invariance and oscillations coming from translation of the domain. To avoid these difficulties, we look for a new formulation taking account of the phase. So it is quite natural to decompose a function $u \in H^1(\Omega)$ as soon it is possible as

$$\forall x \in \Omega,\ u(x) = \rho(x)e^{i\theta(x)}. \tag{2.15}$$

As soon $\rho \in H^1(\Omega) \cap L^\infty(\Omega)$ and $\theta \in H^1(\Omega)$, we have

$$\int_\Omega |(\nabla - iB\mathcal{A}_0)u|^2\ dx = \int_\Omega |\nabla\rho|^2 + |(B\mathcal{A}_0 - \nabla\theta)\rho|^2\ dx. \tag{2.16}$$

Let us define the operator $P^\theta_{\mathcal{A},\Omega}$ by $P^\theta_{\mathcal{A},\Omega}\rho := -\nabla^2\rho + |\mathcal{A} - \nabla\theta|^2\rho$. Then

$$P_{B\mathcal{A}_0,\Omega}(\rho e^{i\theta}) = e^{i\theta}P^\theta_{B\mathcal{A}_0,\Omega}\rho. \tag{2.17}$$

By gauge transform (cf Proposition 1.1), $u = \rho e^{i\theta}$ is an eigenvector with phase θ for $P_{B\mathcal{A}_0,\Omega}$ if and only if ρ is a real-valued eigenvector for $P^\theta_{B\mathcal{A}_0,\Omega}$. So, we are lead to determine

$$\tilde{\mu}(B,\Omega) := \inf_{\theta\in H^1(\Omega),\rho\in H^1(\Omega)\cap L^\infty(\Omega),\rho\neq 0} \frac{\int_\Omega (|\nabla\rho|^2 + \rho^2|B\mathcal{A}_0 - \nabla\theta|^2)\ dx}{\int_\Omega |\rho|^2\ dx}. \tag{2.18}$$

Remark 2.6. *Just by consideration about the domain, the min-max principle shows that*

$$\mu(B,\Omega) \leq \tilde{\mu}(B,\Omega). \tag{2.19}$$

If Ω is smooth and if the modulus ρ of the fundamental state for $P_{B\mathcal{A}_0,\Omega}$ is uniformly bounded from below by a positive constant, then using works of Béthuel-Zheng [4], Bourgain-Brezis-Mironescu [8, 9]

$$\mu(B,\Omega) = \tilde{\mu}(B,\Omega).$$

We can assume weaker conditions about ρ but it is not the main question here.

Although the equality $\mu(B,\Omega) = \tilde{\mu}(B,\Omega)$ is not proved, we use the new formulation and take interest about the discretized formulation (2.20) naturally derived from (2.18)

$$\inf_{(\rho,\theta)\in\mathbb{P}^k(\mathcal{T}_h),\rho\neq 0} \frac{\int_\Omega (|\nabla\rho|^2 + \rho^2|B\mathcal{A}_0 - \nabla\theta|^2)\ dx}{\int_\Omega |\rho|^2\ dx}. \tag{2.20}$$

Performance and robustness of the new formulation (2.20) justify this choice.

Proposition 2.7. *Formulation (2.20) is gauge invariant if the gauge is in the space of the phase's discretization. It is also invariant under translation or rotation of the domain as soon linear functions belong to the discretization'space.*

Proof :
1. Let us consider a magnetic potential $B\mathcal{A}_0 + \nabla\phi$ with $\phi \in \mathbb{P}^k(\mathcal{T}_h)$; Proposition 1.1 says that the eigenvector associated to $P_{B\mathcal{A}_0+\nabla\phi,\Omega}$ is $u_\phi = e^{i\phi}u$ where u is the fundamental state for $P_{B\mathcal{A}_0,\Omega}$. So $(B\mathcal{A}_0+\nabla\phi)-\nabla(\theta+\phi) = B\mathcal{A}_0-\nabla\phi$. Then formulation (2.20) is gauge invariant.
2. According Remark 2.1, $\rho e^{i\theta}$ is an eigenvector for $P_{B\mathcal{A}_0,\Omega}$ if and only if $\rho e^{i(\theta-\eta)}$ is an eigenvector for $P_{B\mathcal{A}_0,\Omega^\eta}$ where Ω^η is deduced from Ω by rotation. Since $\nabla(\theta-\eta) = \nabla\theta$, formulation (2.20) is invariant under rotation of the domain.
3. Let us assume that $k \geq 1$, for that the $\mathbb{P}^k(\mathcal{T}_h)$ discretization contains linear functions. Remark 2.1 gives the eigenvector $e^{i\frac{B}{2}x\wedge t}u(x-t)$ for $P_{B\mathcal{A}_0,\Omega_t}$ where Ω_t is translated from Ω, according to u eigenvector for $P_{B\mathcal{A}_0,\Omega}$. We compute easily $\nabla\left(\frac{B}{2}x\wedge t+\theta\right) = \frac{B}{2}\begin{pmatrix} t_2 \\ -t_1 \end{pmatrix} + \nabla\theta$, so we deduce

$$\inf_{\theta\in\mathbb{P}^k(\mathcal{T}_h)} \int_\Omega |B\mathcal{A}_0 - \nabla\theta|^2\ dx = \inf_{\theta\in\mathbb{P}^k(\mathcal{T}_h)} \int_\Omega \left|B\mathcal{A}_0 - \nabla\left(\frac{B}{2}x\wedge t+\theta\right)\right|^2\ dx.$$

Thus formulation (2.20) is invariant under translation of the domain. □
Formulation (2.20) gives an algorithm to compute numerically $\tilde{\mu}(B,\Omega)$.

Algorithm 2.8.

---

1. *Computation of the mass matrix M.*
2. *Initial choice for ρ normalized and θ.*
3. *Determination of θ by minimization of the functional J_ρ with a conjugate gradient method :*

$$J_\rho(\theta) = \int_\Omega \rho^2(|\nabla\theta|^2 - 2B\mathcal{A}_0\cdot\nabla\theta)\ dx. \tag{2.21}$$

4. *Computation with (2.16) of the energy associated to $\rho e^{i\theta}$.*
5. *Determination of the fundamental state (μ_h,ρ) of $P^\theta_{B\mathcal{A}_0,\Omega}$.*
6. *Reiteration with (ρ,θ) till convergence of the energy μ_h.*

We take again previous examples. We denote by $(\rho_j, \theta_j, \mu_h^j)_{j=0,1,2}$ modulus, phase and energy computed for the mesh $\mathcal{T}_h^j$. For an angular sector cut smoothly, numerical results are presented in Table 2. Figures 5 and 6 give moduli and phases for a magnetic field $B = 30$ and 100 Teslas respectively.

B	Mesh with 138 elements			Mesh with 1328 elements		
	$\mathcal{T}_h^0$	$\mathcal{T}_h^1$	$\mathcal{T}_h^2$	$\mathcal{T}_h^0$	$\mathcal{T}_h^1$	$\mathcal{T}_h^2$
10 Teslas	4.2137	4.2153	4.2149	4.2144	4.2238	4.2166
30 Teslas	12.9965	12.9964	12.9954	12.6075	12.6084	12.6092
50 Teslas	22.6233	22.6232	22.6233	21.0096	21.0101	21.0107
100 Teslas	49.1604	49.1604	49.1605	42.1852	42.1857	42.1858

Table 2: Energy for translated meshes.

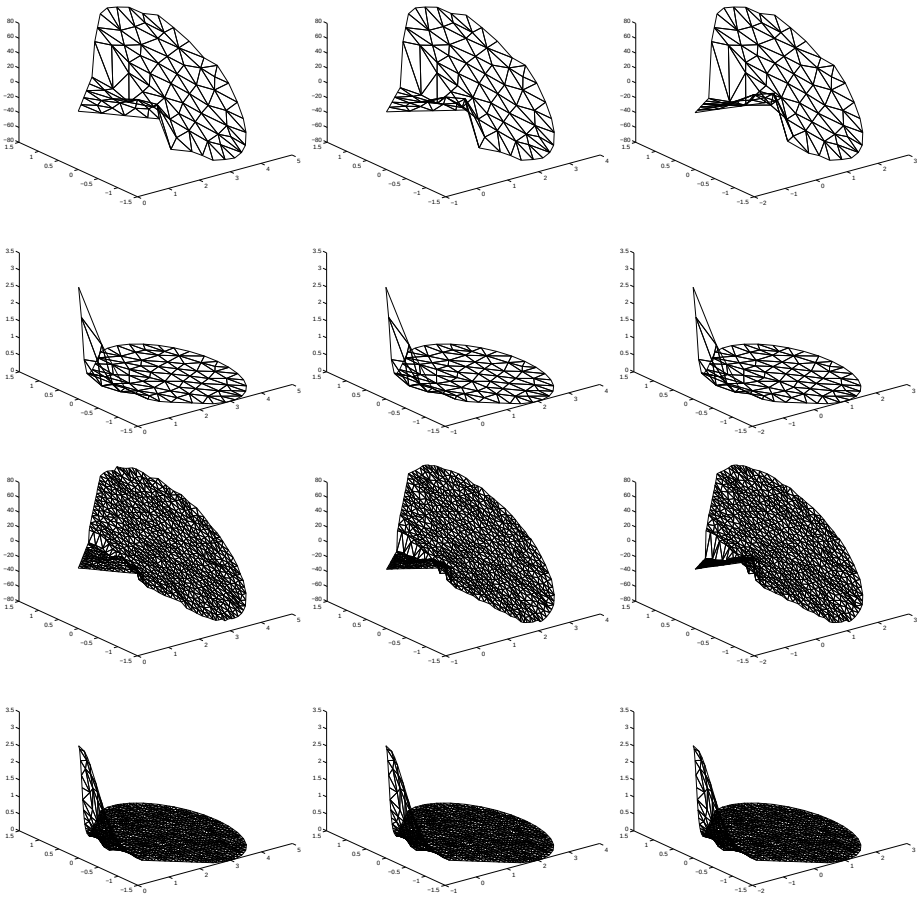

Figure 5: Phase and moduli of eigenvectors in translated meshes, B=30 Teslas.

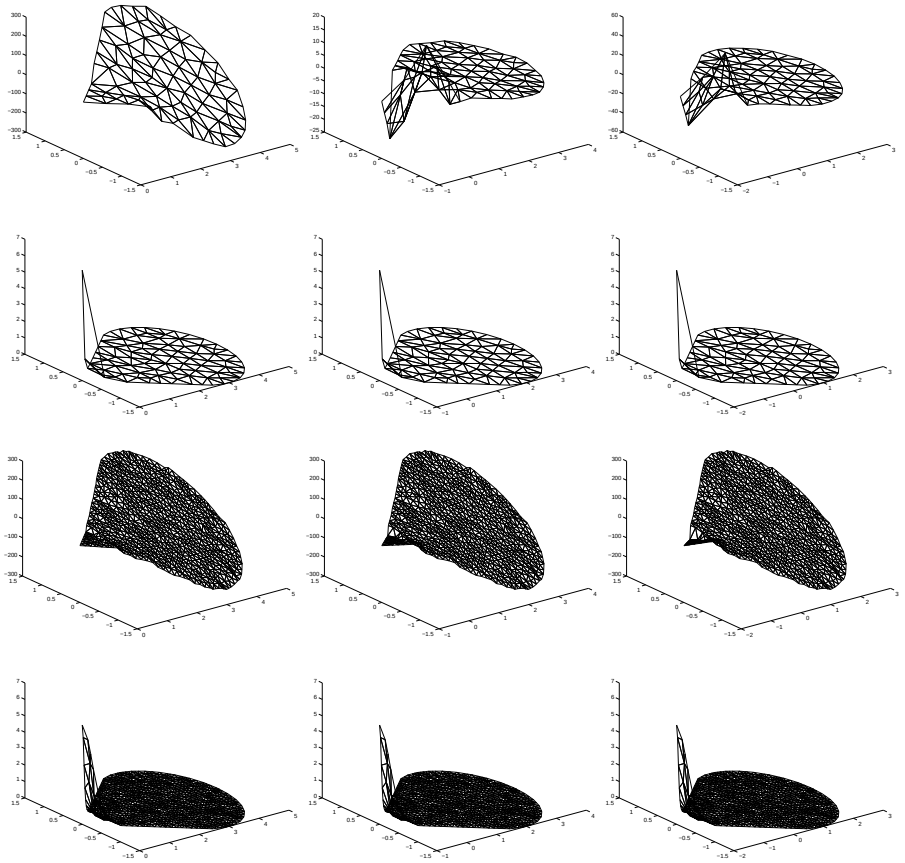

Figure 6: Phase and moduli of eigenvectors in translated meshes, B=100 Teslas.

Let us analyze step by step effects of Algorithm 2.8. At the first step, ρ is random, so we compute a smooth phase θ which is well determined and there is no problem with the conditionment of the functional J_ρ defined in (2.21). Then, we compute the first eigenspace (μ_h, ρ) for $P^\theta_{B\mathcal{A}_0,\Omega}$ with Algorithm 2.3. During the second step, we determine a new phase θ by minimization of J_ρ. We apply a gradient conjugate method initialized with the previous phase. It is important to see that the contribution in $J_\rho(\theta)$ where ρ is close to zero is also very small. That is to say, the phase θ stays quite constant all along iterations where the modulus ρ is very small. So the minimization's problem can be reduced to a smaller area $\Omega \setminus \Omega_\varepsilon$ with $\Omega_\varepsilon = \{\rho < \varepsilon\}$. Obviously, the phase does not have much signification on Ω_ε, since in this area, $\rho e^{i\theta}$ is close to zero. So step by step, the phase will change where the modulus is not too small in order to minimize J_ρ whereas it stays constant elsewhere.
Considering Table 2, it is also interesting to see that the results are coherent together : if you look at results associated to one size of triangulation, energies for every meshes are quite the same. Differences between coarse and fine meshes

come from the bad accuracy for a coarse mesh.
We remark that the concentration of the eigenvector in the corner is faster and faster when the magnetic fiel B is increasing as illustrated in Figures 5 and 6. We also notice that this method is still robust and available for intense magnetic field whereas the standard method was already unefficient for magnetic field $B = 30$ Teslas.

We now consider a triangular domain. As before, we mesh the triangle and translate this mesh. We want to observe the effect of a translation. With the previous notations, Remark 2.1 and Relation (2.14) show that

$$\theta_j - \theta_0 = -\frac{B}{2} x \wedge \mathbf{t_j} = \frac{B}{2} j x_2 \text{ with } \mathbf{t_j} = (j, 0),\ j = 1, 2. \tag{2.22}$$

So the difference of phase between two translated meshes is constant according x_1-coordinates and linear according x_2-coordinates. Figure 7 illustrates the

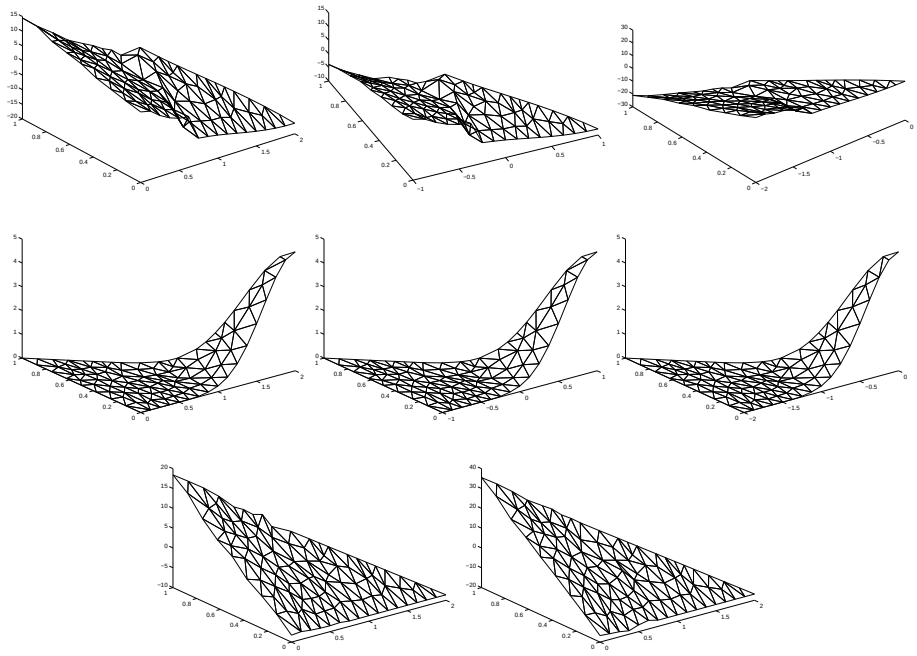

Figure 7: Arguments, moduli and phase'differences for eigenvectors in translated meshes, $B = 50$ Teslas.

application of Algorithm 2.8 : the first, second and third lines give respectively θ_0, θ_1, θ_2 ; ρ_0 , ρ_1, ρ_2 and $\theta_1 - \theta_0$, $\theta_2 - \theta_0$. As it was explained in (2.22), we observe that the difference $\theta_j - \theta_0$ is constant according x_1-coordinates and linear according x_2-coordinates. If we look at the slope of the curve, we find exactly the slope given by (2.22), that is to say

$$\partial_{x_1}(\theta_j - \theta_0) = 0 \text{ and } \partial_{x_2}(\theta_j - \theta_0) = \frac{B}{2} j.$$

Thus we find an algorithm invariant under translation, rotation of the domain and gauge invariant. The Algorithm 2.8 is particularly robust and powerful because it is still available for intense magnetic field for which the concentration of the eigenvector is essentially in a couple of elements of the triangulation (see e. g. Figure 6).

We notice also that the order of the determination of arguments and moduli is rather important : if in Algorithm 2.8, we choose to determine firstly the modulus and after, we minimize the functional J_ρ to find the phase θ, then we keep similar problems as in standard method described in Section 2.3. Indeed, the problem of minimization of J_ρ is badly conditioned as soon ρ is very small in some areas of the domain and it is the case for the modulus of the fundamental state.

To validate this modelization, we have to compute error between continuous and discrete solutions. For this, we construct localized a posteriori error estimates. This technique is well adapted to the problem since the eigenvector is localized and it is probably not necessary to lose time of computation in some areas of the domain. Theoretical study suggests that the boundary and more precisely corners play the most important role of the domain and mesh-refinement techniques can use these informations to perform computations.

3 A posteriori error estimate

3.1 Presentation

Since the last algorithm give us a numerical solution of the initial problem (1.6), we want to determine the gap between the exact solution and the approximate solution given by this algorithm. We propose here a criterion which permits to know, using only computed numerical solution and data of the problem, if the numerical solution is close to the exact solution with a prescribed accuracy. In this aim, we have constructed a posteriori error estimates. The main advantage of such a criterion is that we compute at each element of the mesh the local error between exact and numerical solution. If the error is too large, we refine this area to improve the accuracy. Let us recall some notations before giving the main theorem about these estimates. This section is detailed in [6].

3.2 Notations

We use the same notations as Verfürth [27], p. 7-8. Let $\mathcal{T}_h$, $h > 0$ be a family of triangulations of Ω filling the following conditions :

1. Any two triangles in $\mathcal{T}_h$ share at most a common edge or a common vertex.
2. The minimal angle of all triangles in the whole family $\mathcal{T}_h$ is bounded from below by a strictly positive constant.

Let $\mathbb{P}^2(\mathcal{T}_h)$ be the space of all continuous, quadratic finite element functions corresponding to $\mathcal{T}_h$. We consider the following eigenvalue problem

$$\text{Find } (\mu_h, u_h) \in \mathbb{R} \times \mathbb{P}^2(\mathcal{T}_h) \text{ with the smallest } \mu_h \text{ s.t.}$$

$$\forall v_h \in \mathbb{P}^2(\mathcal{T}_h),\ \left\{ \begin{array}{rcl} \int_\Omega \nabla_{\mathcal{A}} u_h \cdot \overline{\nabla_{\mathcal{A}} v_h} & = & \mu_h \int_\Omega u_h \overline{v}_h, \\ \int_\Omega |u_h|^2 & = & 1, \end{array} \right. \tag{3.1}$$

For any element T of the triangulation $\mathcal{T}_h$, we denote by $\mathcal{E}(T)$ and $\mathcal{N}(T)$ the set of its edges and vertices respectively and we define

$$\mathcal{E}_h := \bigcup_{T \in \mathcal{T}_h} \mathcal{E}(T),\ \mathcal{N}_h := \bigcup_{T \in \mathcal{T}_h} \mathcal{N}(T).$$

For $T \in \mathcal{T}_h$ and $E \in \mathcal{E}_h$, we define h_T and h_E their diameter and length, respectively. We assume $h_T,\ h_E < h$. We remark that if the triangulation satisfies the condition 2, then the ratios $\frac{h_T}{h_E}$ and $\frac{h_T}{h_{T'}}$ are bounded from below independently of h for every $T,\ T' \in \mathcal{T}_h$ such that $\mathcal{N}(T) \cap \mathcal{N}(T') \neq \emptyset$, and for every $E \in \mathcal{E}(T)$.
We split $\mathcal{E}_h$ as follow

$$\mathcal{E}_h = \mathcal{E}_{h,\Omega} \cup \mathcal{E}_{h,\Gamma},$$

with

$$\mathcal{E}_{h,\Omega} := \{E \in \mathcal{E}_h | E \subset \Omega\},\ \mathcal{E}_{h,\Gamma} := \{E \in \mathcal{E}_h | E \subset \Gamma\},$$

For any $E \in \mathcal{E}_h$, we define $\omega_E := \bigcup_{E \in \mathcal{E}(T')} T'$ the set of elements which admit E as edge. For any edge $E \in \mathcal{E}_h$, we associate a unit vector n_E (equal to ν if $E \subset \Gamma$). For any $E \in \mathcal{E}_{h,\Omega}$ and $\phi \in L^2(\omega_E)$ such that $\phi_{|_{T'}}$ is continuous on T' for any $T' \subset \omega_E$, we denote by $[\phi]_E$ the jump of ϕ across E in the direction n_E. We also define the space

$$X = \mathbb{R} \times H^1_{\mathcal{A}}(\Omega) \text{ and } X_h = \mathbb{R} \times \mathbb{P}^2(\mathcal{T}_h). \tag{3.2}$$

For any $(\mu, u),\ (\lambda, v) \in X$, we define

$$||(\mu, u)||_X := \{|\mu|^2 + ||u||^2_{H^1_{\mathcal{A}}(\Omega)}\}^{1/2}, \tag{3.3}$$

$$\langle F(\mu, u), (\lambda, v)\rangle := \text{ Re } \int_\Omega \left(\nabla_{\mathcal{A}} u \cdot \overline{\nabla_{\mathcal{A}} v} - \mu u \overline{v}\right) + \lambda \left(\int_\Omega |u|^2 - 1\right). \tag{3.4}$$

Our goal is to find $(\mu, u) \in X$ and $(\mu_h, u_h) \in X_h$ such that μ and μ_h are the smallest and

$$\forall (\lambda, v) \in X, \quad \langle F(\mu, u), (\lambda, v)\rangle = 0, \tag{3.5}$$

$$\forall (\lambda_h, v_h) \in X_h, \quad \langle F(\mu_h, u_h), (\lambda_h, v_h)\rangle = 0. \tag{3.6}$$

3.3 A priori error estimate

By using spectral decomposition, we obtain first informations about the gap between the continuous and the discrete solution

Theorem 3.1. *There exists a constant C such that for (μ, u) and (μ_h, u_h) solutions of problems (3.5) and (3.6) respectively where μ and μ_h are the smallest eigenvalues of the continuous and discrete operators, the following upper bounds hold*

$$\begin{array}{rcl} ||u - u_h||_{H^1_{\mathcal{A}}(\Omega)} & \leq & Ch, \\ |\mu - \mu_h| & \leq & Ch^2. \end{array}$$

Of course, this result gives us global information but we are unable to use theses estimates to know where the computation is not accurate. To solve this problem, we now introduce an a posteriori error estimate and explain the great advantage of such tools.

3.4 A posteriori error estimate

We define the a posteriori error estimator for all $T \in \mathcal{T}_h$

$$\eta_T^2 := h_T^2 \int_T \left| -\nabla_{\mathcal{A}}^2 u_h - \mu_h u_h \right|^2 + \sum_{E \in \mathcal{E}(T) \cap \mathcal{E}_{h,\Omega}} h_E \int_E \left| [n_E \cdot \nabla_{\mathcal{A}} u_h]_E \right|^2 . \quad (3.7)$$

As we see in the following theorem, the estimator η_T has a fundamental role to see if we are close to the exact solution or not and to increase accuracy of the numerical solution.

Theorem 3.2. *Let $(\mu, u) \in X$ and $(\mu_h, u_h) \in X_h$ be respectively a solution for the problem (3.5) and the problem (3.6) such that μ and μ_h are the smallest eigenvalues of the continuous and discrete operators. Then, there exist $h_0 > 0$ and constants c_1, c_2 which depend only on the regularity parameter of the triangulation such that for all $h \leq h_0$:*

$$|\mu - \mu_h| + ||u - u_h||_{H^1_{\mathcal{A}}(\Omega)} \leq c_1 \left\{ \sum_{T \in \mathcal{T}_h} \eta_T^2 \right\}^{1/2}, \quad (3.8)$$

$$\left\{ \sum_{T \in \mathcal{T}_h} \eta_T^2 \right\}^{1/2} \leq c_2 \{ |\mu - \mu_h| + ||u - u_h||_{H^1_{\mathcal{A}}(\Omega)} \}. \quad (3.9)$$

Estimators give the way to improve numerical results obtained by Algorithm 2.8 by joining it with mesh-refinement techniques since Theorem 3.2 establishes a kind of norm's equivalence between $|\mu - \mu_h| + ||u - u_h||_{H^1_{B\mathcal{A}_0}(\Omega)}$ and $\left\{ \sum_{T \in \mathcal{T}_h} \eta_T^2 \right\}^{1/2}$.

3.5 Applications to mesh-refinement techniques

Let us consider Theorem 3.2. Let us give a tolerance level ε. If the local estimator η_T at the element T of the triangulation is higher than ε, then

$$\varepsilon \leq \eta_T \leq \left\{ \sum_{T \in \mathcal{T}_h} \eta_T^2 \right\}^{1/2} \leq c_2 \left(|\mu - \mu_h| + ||u - u_h||_{H^1_{B\mathcal{A}_0}(\Omega)} \right).$$

So, forgetting the constant c_2, the gap between numerical and exact solution is higher than ε. So the criterion $\eta_T > \varepsilon$ means that the numerical solution is badly computed on T and it is needed to refine this element. By this way, we deduce an algorithm to refine locally mesh and improve numerical solution.

Algorithm 3.3.

1. *Data of an initial mesh* $\mathcal{T}_{h,0}$ *and a tolerance level* ε.
2. *Computation of a solution* $(\mu_{h,0}, \rho_{h,0}e^{i\theta_{h,0}})$ *with Algorithm 2.8.*
3. *Computation of a posteriori error estimator* $(\eta_T)_{T\in\mathcal{T}_{h,0}}$ *by (3.7) and of the norm* η *with* $\eta^2 = \sum_{T\in\mathcal{T}_{h,0}} \eta_T^2$.
4. *While* $\eta > \varepsilon$:
   - *Construction of a new mesh* $\mathcal{T}_{h,1}$ *deduced from the previous mesh* $\mathcal{T}_{h,0}$ *by refining elements* $T \in \mathcal{T}_{h,0}$ *such that* $\eta_T > \frac{\varepsilon}{\sqrt{\text{Card } T}}$.
   - *Interpolation of* $\rho_{h,0}$ *and* $\theta_{h,0}$ *defined on* $\mathcal{T}_{h,0}$ *to* $\mathcal{T}_{h,1}$.
   - *Computations of the eigenspace on* $\mathcal{T}_{h,1}$ *using Algorithm 2.8 initialized with the interpolations of* $\rho_{h,0}$ *and* $\theta_{h,0}$.

We take again the example of the smoothly cut angular sector and we apply Algorithm 3.3 with a magnetic field $B = 30$ Teslas. Table 3 gives informations for each refinement. The convergence of error estimates and of eigenvalues are precised in Figure 8. Figure 9 illustrates the mesh after six refinements and also gives the phase and the modulus computed according to Algorithm 2.8.

refinement	number of elements	number of degrees of freedom	η	μ_h
1	38	101	38.993385	15.572444
2	102	235	22.828768	13.815911
3	206	459	9.037603	12.826912
4	394	855	5.857042	12.670129
5	800	1699	2.240146	12.638226
6	1726	3593	0.792354	12.628898
7	3807	7826	0.272165	12.627361
8	8219	16742	0.104900	12.626788
9	15517	31446	0.060877	12.626605

Table 3: Estimates for an adaptive refinment method, $B = 30$ Teslas.

During refinements, estimates of the phase are not accurate due to a very easy interpolation : let us consider a phase θ_0 defined on a mesh $\mathcal{T}_{h,0}$. We interpolate it to θ_1 in the refined mesh $\mathcal{T}_{h,1}$ by this way : the value of θ_1 in a degree of freedom in an element $T_1 \in \mathcal{T}_{h,1}$ is the value of θ_0 in a point of $T_0 \in \mathcal{T}_{h,0}$ such that $T_1 \subset T_0$. This very easy interpolation does not perturb too much our accuracy because the modulus is very small on these areas. We observe that the refinement takes place essentially near the corner and also near the boundary. This is in perfect agreement with results of localization announced by [5, 7].

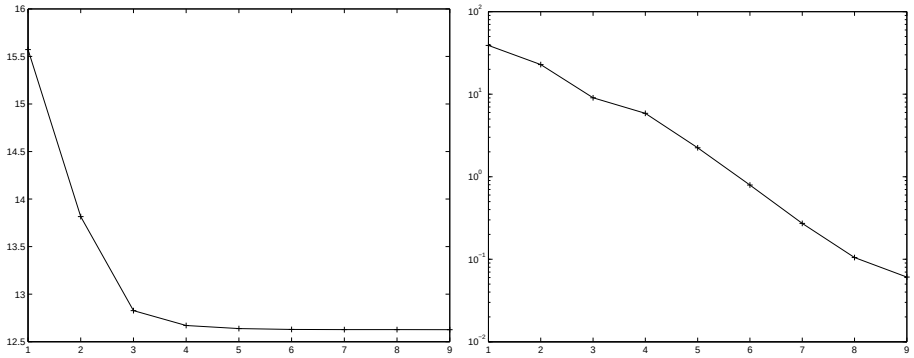

Figure 8: Convergence of eigenvalues and a posteriori error estimates according to the number of refinements, $B = 30$ Teslas.

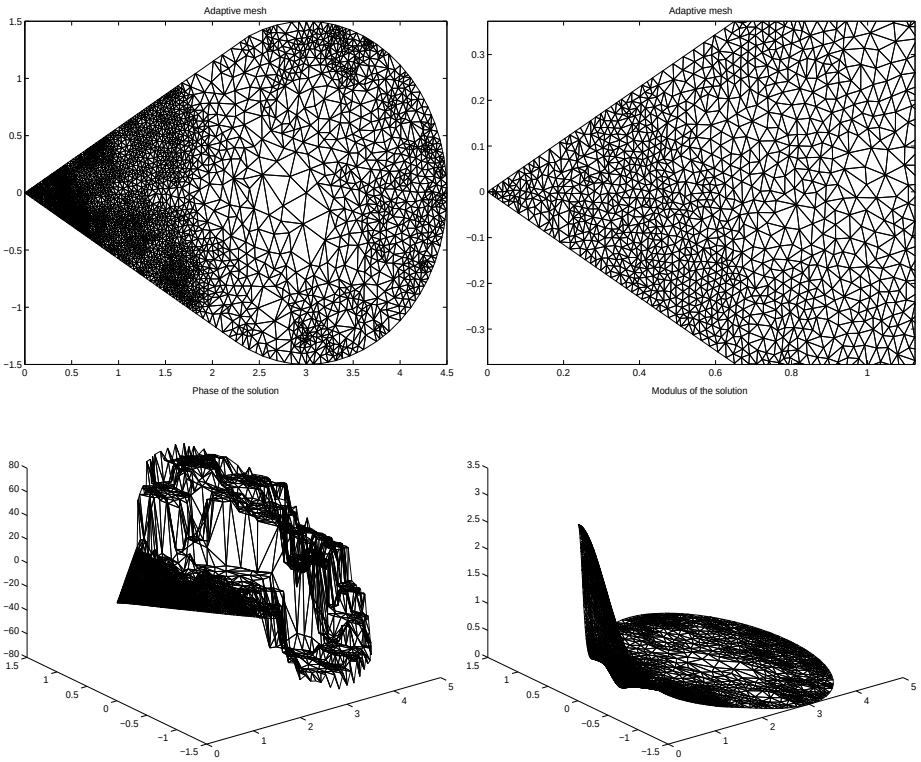

Figure 9: Solution for the sixth refinment.

Let us now compare adaptive mesh refinement and uniform mesh refinement. We apply Algorithm 2.8 on uniform meshes for a magnetic field $B = 30$ Teslas. Results are presented in Table 4. Figures 10 and 11 compare convergence for uniform and adaptive mesh refinements with magnetic field respectively equal to 30 and 100 Teslas. An adaptative mesh refinement is more powerful and

faster than an uniform method. Its power and robustness becomes bigger and bigger when the magnetic field is increasing.

refinement	number of elements	number of degrees of freedom	η	μ_h
1	38	101	39.711605	15.569330
2	48	125	22.754814	13.816984
3	70	171	14.493879	13.440501
4	193	428	8.227542	12.826351
5	522	1113	4.960995	12.687395
6	1349	2790	2.059195	12.641156
7	3593	7350	0.772448	12.630521
8	9583	19448	0.279150	12.627457

Table 4: Estimates for a uniform mesh refinement.

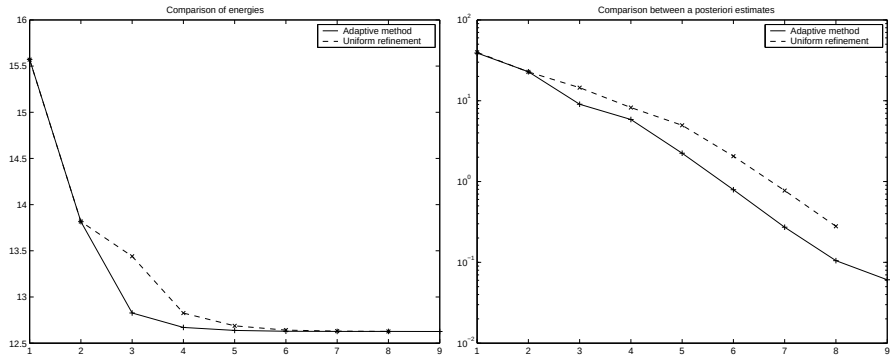

Figure 10: Comparison of convergence between adaptive and uniform meshes, $B = 30$ Teslas.

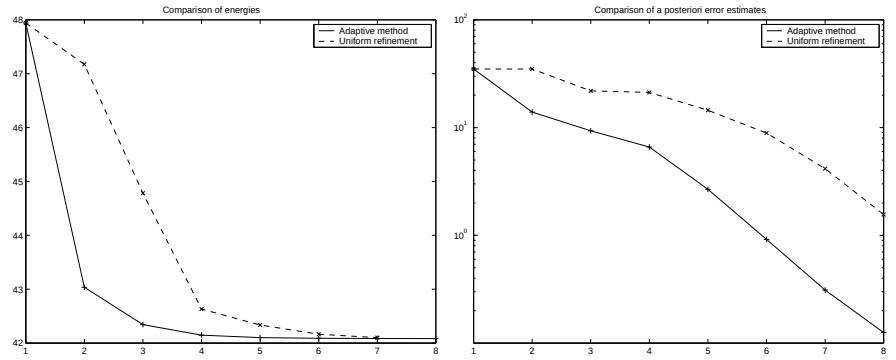

Figure 11: Comparison of convergence between adaptive and uniform meshes, $B = 100$ Teslas.

4 Applications

As we have already seen, Algorithm 3.3 is well adapted to the problem and we can find accurate numerical solution for the problem (1.6). As we explain in introduction in (1.10), it is very important to determine with accuracy the bottom of the spectrum for the operator $P_{\mathcal{A}_0,\Omega_\alpha}$ because informations about this operator are usefull to localize superconductivity in general domains. This operator is studied theoretically in [5, 7]. Let us just recall a couple of estimates obtained for $\mu(\alpha)$

$$
\begin{aligned}
&(1) \quad \forall \alpha \in]0, 2\pi[,\ \mu(\alpha) \leq \Theta_0,\\
&(2) \quad \forall \alpha \in]0, \pi[,\ \mu(\alpha) \geq \Theta_0 \frac{\alpha}{\pi},\\
&(3) \quad \forall \alpha \in]0, 2\pi[,\ \mu(\alpha) \leq \frac{\alpha}{\sqrt{3}},\\
&(4) \qquad \lim_{\alpha \to 0} \frac{\mu(\alpha)}{\alpha} = \frac{1}{\sqrt{3}}.
\end{aligned}
$$

Since Ω_α is invariant under dilatation, we know according Remark 2.1 that $\mu(B, \Omega_\alpha) = B\mu(\alpha)$. We now apply Algorithm 3.3 to estimate $\mu(\alpha)$. For this, we use the previous cut-off angular sector : we consider an angular sector and we cut it by a piece of circle so that the boundary is still smooth, except at the corner. The bottom of the spectrum does not change (with an exponentially small error) if the cutt-off is quite far the corner. The smooth cut-off does not introduce new point of superconducting localization and does not change the superconducting behavior of the sample. Numerical estimates of $\mu(\alpha)$ are described in Figure 12. We note that numerical estimates are in perfect agreement with estimates (1), (2), (3) and (4) : the asymptotics near zero is conserved and numerical results tend to convince us that μ is increasing from $]0, \pi]$ onto $]0, \Theta_0]$.

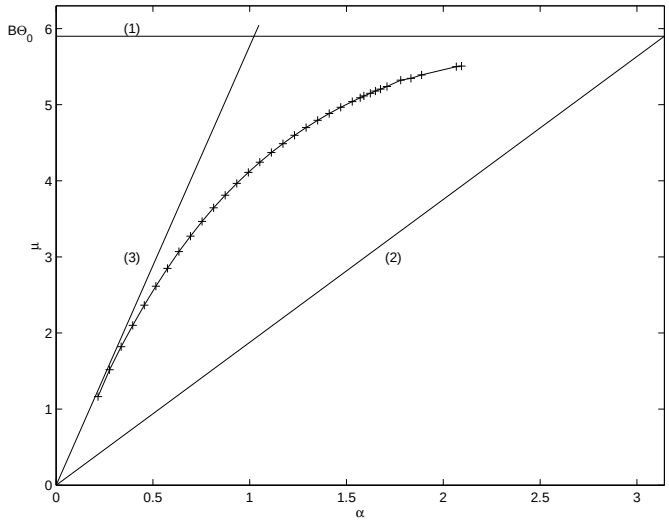

Figure 12: Theoretical and numerical estimates of $\mu(\alpha)$, $B = 10$ Teslas.

We now briefly treat three general domains for which we apply Algorithm 3.3. It is interesting to observe in Figure 13 that the localization takes place at one

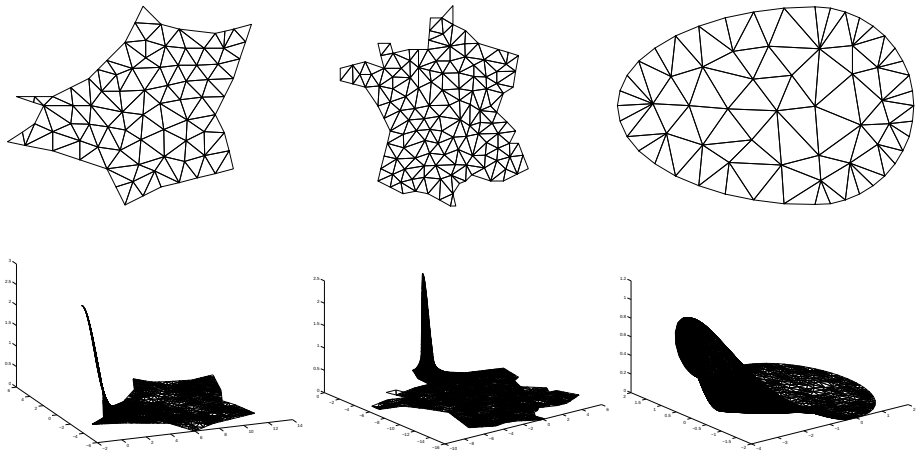

Figure 13: Superconductivity in general domains.

corner where the angle is the smallest. We notice that the third domain is smooth : it is one half circle with one half ellipse and we illustrate results obtained by Helffer-Morame [16] which mentionned that the fundamental state is localized at points of the boundary where the curvature is maximal.

5 Conclusion

We proposed here a robust and powerful method to compute fundamental state associated to the Schrödinger operator with magnetic field and join this method with an adaptative mesh refinement technique deduced from the construction of a posteriori error estimate. Thus, we propose some estimates of $\mu(\alpha)$, the bottom of the spectrum for the Schrödinger operator with a constant magnetic field in an α-angular sector. These numerical estimates coupled with results of [7] let suggest that the first eigenfunction of the Schrödinger operator with magnetic field is exponentially localized in the smallest corners.
We hope to come back in an other paper for the localization of the superconductivity in domain with several minimal angles.

Acknowledgements
I would like to thank François Alouges for his optimism and his help.

References

[1] F. Alouges and V. Bonnaillie, Analyse numérique de la supraconductivité, C. R. Acad. Sci. **337-8,** (2003) p. 543-548.

[2] C. Bernardi, B. Métivet, Indicateurs d'erreur pour l'équation de la chaleur, Rev. Eur. Elem. Finis **9-4,** (2000) p. 423-438.

[3] A. Bernoff and P. Sternberg, Onset of superconductivity in decreasing fields for general domains, J. Math. Phys. **39-3,** (1998) p. 1272-1284.

[4] F. Bethuel et X. M. Zheng, Sur la densité des fonctions régulières entre deux variétés dans les espaces de Sobolev, C. R. Acad. Sci. Paris Sér. I Math. **303-10,** (1986) p. 447-449.

[5] V. Bonnaillie, On the fundamental state for a Schrödinger operator with magnetic field in a domain with corners, C. R. Acad. Sci. **336-2,** (2003) p. 135-140.

[6] V. Bonnaillie, A posteriori error estimator for the eigenvalue problem associated to the Schrödinger operator with magnetic field, submitted (april 2003).

[7] V. Bonnaillie, On the fundamental state energy for a Schrödinger operator with magnetic field in domains with corners, submitted (may 2003).

[8] J. Bourgain and H. Brezis and P. Mironescu, On the structure of the Sobolev space $H\mathrm{Sp}\,1/2$ with values into the circle, C. R. Acad. Sci. Paris Sér. I Math. **331-2,** (2000) p. 119-124.

[9] J. Bourgain and H. Brezis and P. Mironescu, Limiting embedding theorems for $W\mathrm{Sp}\,s,p$ when $s \uparrow 1$ and applications, J. Anal. Math. **87,** (2002) p. 77-101.

[10] D. Braess , *Finite elements*, (Cambridge University Press, 2001).

[11] F. Brosens, J. T. Devreese, V. M. Fomin and V. V. Moshchalkov, Superconductivity in a wedge : analytical variational results, Solid State Comm. **111-12,** (1999) p. 565-569.

[12] P. Clément, Approximation by finite element functions using local regularization, R. A. I. R.O., **R-2**, (1975) p. 77-84.

[13] V. M. Fomin, J. T. Devreese and V. V. Moshchalkov, Surface superconductivity in a wedge, Europhys. Lett. **42-5**, (1998) p. 553-558.

[14] P. G. de Gennes, *Superconductivity in metals and Alloys* (Addison Wesley, 1989).

[15] B. Helffer and A. Mohamed, Semiclassical analysis for the ground state energy of a Schrödinger operator with magnetic wells, J. of Functional Analysis **138-1,** (1996) p. 40-81.

[16] B. Helffer and A. Morame, Magnetic bottles in connection with superconductivity, J. of Functional Analysis **185,** (2001) p. 604-680.

[17] B. Helffer and X. P. Pan, Upper critical field and location of surface nucleation of superconductivity, Ann. I. H. Poincaré **AN 20,** 1 (2003) p. 145-181.

[18] K. Hornberger and U. Smilansky, The boundary integral method for magnetic billiards, J. Phys. A : Math. Gen. **33,** (2000) p. 2829-2855.

[19] H-T. Jadallah, The Onset of superconductivity in a domain with a corner, Ph. D. Indiana University (2001).

[20] H-T. Jadallah, The Onset of superconductivity in a domain with a corner, J. Math. Phys. **42-9**, (2001) p. 4101-4121.

[21] D. Saint-James and P. G. de Gennes, Onset of Superconductivity in decreasing fields. Phys. Let. **7-5**, (1963) p. 306-308.

[22] K. Lu and X-B. Pan, Estimates of the upper critical field for the Ginzburg-Landau equations of superconductivity, Physica D **127,** (1999) p. 73-104.

[23] K. Lu and X-B. Pan, Gauge invariant eigenvalue problems on $\mathbb{R}^2$ and $\mathbb{R}^2_+$, Trans. A. M. S. **352,** (2000) p. 1247-1276.

[24] X. B. Pan, Upper Critical Field for superconductors with edges and corners, Calc. Var. Partial Differential Equations **14,** (2002) p. 447-482.

[25] V. A. Schweigert and F. M. Peeters, Influence of the confinement geometry on surface superconductivity, Phys. Rev. B **60-5,** (1999) p. 3084-3087.

[26] M. Tinkham, *Introduction to superconductivity* (McGraw Hill, 1996).

[27] R. Verfürth, *A review of a posteriori error estimation and adaptative mesh rafinement technique* (Wiley Teubner, 1996).